Volume 1 | Number 1 | Jan 2013 | Pages 1–100

RSC Advances

www.rsc.org/advances

ROYAL SOCIETY OF CHEMISTRY

www.rsc.org/advances

RSC Advances - Manuscript ID RA-ART-04-2014-002957

Lithium ferrite (Li$_{0.5}$Fe$_{2.5}$O$_4$) nanoparticles as anode for lithium ion batteries

Table of content
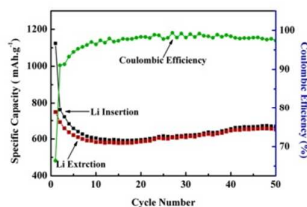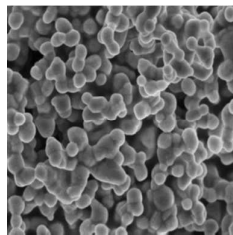
Sentence: Lithium ferrite (Li$_{0.5}$Fe$_{2.5}$O$_4$) nanoparticles are excellent anode materials for lithium ion batteries.

ARTICLE TYPE

Lithium ferrite ($Li_{0.5}Fe_{2.5}O_4$) nanoparticles as anode for lithium ion batteries

Hong Zeng [a], Tao Tao[b], Ying Wu[a], Wen Qi [a], Chunjiang Kuang[a], Shaoxiong Zhou[a] and Ying Chen[b],*

$Li_{0.5}Fe_{2.5}O_4$ nanoparticles of about 80 nm were synthesized through hydrothermal method, followed by a solid state reaction between $LiOH \cdot H_2O$ and Fe_2O_3. The $Li_{0.5}Fe_{2.5}O_4$ nanoparticles exhibit a remarkable high capacity (up to 1124
10 **$mAhg^{-1}$), a good cycle stability (650 $mAhg^{-1}$ after 50 cycles) and excellent coulombic efficiency.**

Introduction

Lithium-ion battery has been one of the most important and
15 widely used rechargeable power sources because of its high energy density, long lifespan, and environmentally friendly [1-2]. Graphite is currently used as the commercial anode material. However, graphite-based anodes has a low theoretical capacity of around 372 mAh g^{-1}, which cannot satisfy the increasing demand
20 for high energy density lithium-ion battery [3]. Therefore, it is essential to develop new anodes made from low cost and non-toxic electrode materials of higher energy density and better cycling stability.

Lithium ferrite ($Li_{0.5}Fe_{2.5}O_4$) is an important transition metal
25 spinel oxide with the advantage of low cost, environmental friendliness, and easy fabrication [4-5]. It has been extensively studied for various technological applications such as the components of microwave devices and potential cathode materials in lithium batteries [6-10]. Iron-based compounds
30 including $LiFeO_2$ and Fe_xO_y have high theoretical capacities and are non-toxic, environmentally friendly, and low costs [11-13]. $Li_{0.5}Fe_{2.5}O_4$ materials have not been used as the anode for the Li-ion battery. In this paper, we report the synthesis of $Li_{0.5}Fe_{2.5}O_4$ nanoparticles through hydrothermal and a solid state reaction
35 processes. The $Li_{0.5}Fe_{2.5}O_4$ nanoparticles exhibit good cyclability and high reversible lithium storage capacity.

Experimental

Materials synthesis

40 The $LiFeO_4$ nanoparticles were produced by a two-step procedure involving hydrothermal and subsequent heating treatments. The commercial $FeCl_3$ (purity 98%), and $NH_4H_2PO_4$ (purity 98%) were dispersed into water under vigorous magnetic stirring (300 rpm), and then transferred into a Teflon-lined
45 stainless steel autoclave. The autoclave was heated at 220 °C for 1 h. After cooling down to room temperature naturally, the precipitate was collected by centrifugation and washed with distilled water first and then absolute ethyl ethanol for several times. The obtained samples were mixed with $LiOH \cdot H_2O$ (purity
50 98%,) in ethanol to form a homogenous mixture, and dried at the room temperature. Finally, the dried sample was heated at

different temperatures for 10 h under the ambient atmosphere.

Materials characterization

The morphology and structure of the powders were determined using a field-emission scanning electron microscope (SEM, FEI NOVA-450) and transmission electron microscope (TEM, PHILIPS TECNAI F30). The crystalline structure of the materials were measured using X-ray diffraction (XRD, BRUKER D8) using Cu K_α radiation at 40 KV and 40 mA with a step size of 0.02^o and step time of 5 seconds. Sample surface area was measured using the Brunauer–Emmett–Teller (BET) method with a Quanta Autosorb-iQ2-MP-ANG-VP instrument.

Electrochemical measurements

The electrodes were prepared using a mixture of active material, carbon black (AB), and polyvinylidene fluoride (PVDF) at a weight ratio of 70:20:10, dispersed in N-methylpyrrolidone (NMP) to form homogenous slurry. The slurry was spread onto a copper foil and dried at 110 °C for 20 h in a vacuum oven. After drying, the electrode foils were pressed and then punched into a circular shape. Electrochemical experiments were carried out using CR2025-type coin cells assembled in an argon-filled glove box. Li metal foil was used as a counter electrode and 1 M solution of $LiPF_6$ in ethylene carbonate (EC) and dimethyl carbonate (DMC) (1:1, v/v) was selected as the electrolyte. The galvanoscope charge-discharge tests were conducted at a current density of 100 mAg^{-1} and cut-off voltages of 0.01 and 3 V at room temperature using an automatic Land battery instrument. Cyclic voltammetry (CV) was also conducted on the VMP3 electrochemical workstation (BIO-LOGIC SA France) between voltages 0.01 and 3.0 V at a scan rate of 0.1 mV s^{-1}.

Results and discussion

Fig.1a shows the typical SEM and inserted TEM images of the sample after annealing at 600°C for 10 h. It can be seen that the powder contains spherical particles and the inserted TEM image confirms nanocrystalline structure of the particles. The size distribution in Fig.1b shows a diameter around 80nm, which is consistent with a large surface area of the sample at 19.5 m^{2}g^{-1}.
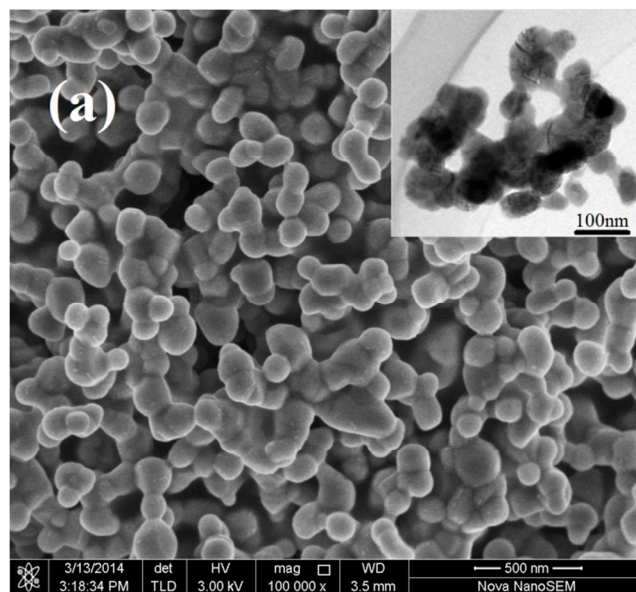

Figure. 1 SEM and TEM images (a), and particle size distribution (b) of the sample obtained from Fe_2O_3 and LiOH•H_2O after heating at 600 °C,

The XRD pattern of the sample is shown in Fig. 2. The diffraction peaks can be indexed to a crystalline structure of spinel $Li_{0.5}Fe_{2.5}O_4$ (PDF No. 74-1911), which belongs to the space group P4132, and no other impurity peaks can be observed.

Fig. 3a shows the CV curves of the $Li_{0.5}Fe_{2.5}O_4$ anode.

During the cathodic polarization in the first cycle, a spiky peak was observed at 0.97 V corresponding to the complete reduction of iron from Fe^{3+} to Fe^{0+} [14, 15]:

$$2Li_{0.5}Fe_{2.5}O_4 + 15Li^+ + 15e^- \rightarrow 5Fe^0 + 8Li_2O \qquad (1)$$
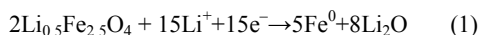
On the other hand, in the anodic polarization process, a broad peak was recorded at about 1.05 V corresponding to the oxidation of Fe^0 to Fe^{2+} and further oxidization to Fe^{3+} [16, 17]:

$$2Fe^0 + 2Li_2O \leftrightarrow 2Fe^{II}O + 4Li^+ + 4e^- \qquad (2)$$
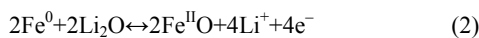
After the second cycle, the CV curves are very stable for the $Li_{0.5}Fe_{2.5}O_4$ nanoparticles electrode indicating enhanced stability during the lithiation and delithiation processes.

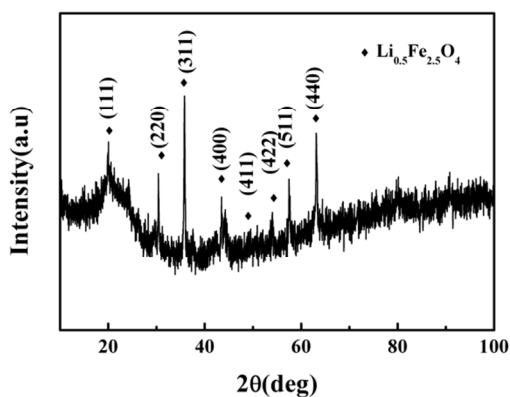**Figure 2.** XRD pattern of samples obtained at 600°C from Fe_2O_3 and LiOH•H_2O

Fig. 3b shows the corresponding discharge-charge voltage profiles of $Li_{0.5}Fe_{2.5}O_4$ nanoparticles. During the first discharge, a long plateau appears at about 0.8 V versus Li/Li^+, indicating the complete reduction of iron from Fe^{3+} to Fe^{0+}. For the charge curves, a wide slope located at 1.5-2.0 V is observed, corresponding to the oxidation of Fe^0 to Fe^{2+}, with part of the Fe further oxidized to Fe^{3+}. The electrochemical behavior is consistent with the results of the CV measurement. The first and second discharge capacity of $Li_{0.5}Fe_{2.5}O_4$ electrode are 1124 mAhg^{-1} and 746mAhg^{-1}, respectively. The initial capacity loss of

the $Li_{0.5}Fe_{2.5}O_4$ nanoparticles electrode is 33.7% and could result from the formation of a solid electrolyte interface (SEI) on the iron oxide surface during the first lithium insertion process [18]. Fig. 3c shows the cycling performance of the $Li_{0.5}Fe_{2.5}O_4$ anode, indicating a reversible capacity of about 650mAhg^{-1} after 50 cycles. The coulombic efficiency of $Li_{0.5}Fe_{2.5}O_4$ nanoparticles is above 96% after 10 cycles.
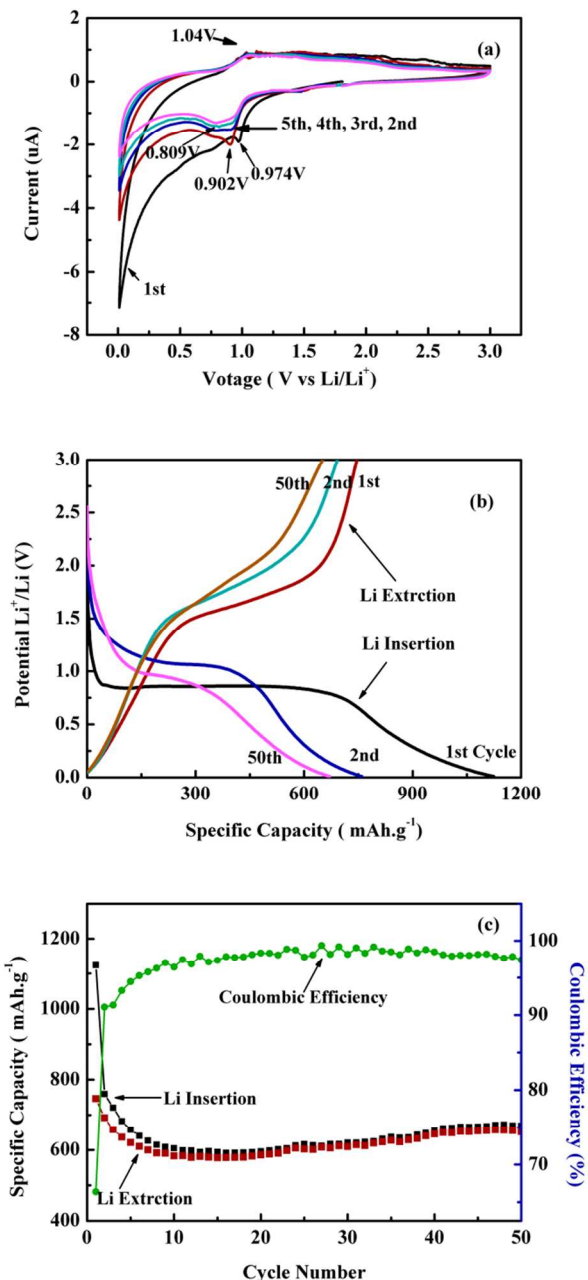

Figure 3 (a) Cyclic voltammentry (CV) curves, (b) discharge-charge curves, and (c) cycling performances of $Li_{0.5}Fe_{2.5}O_4$ nanoparticles.

The typical first discharge-charge curves of the $Li_{0.5}Fe_{2.5}O_4$ nanoparticles electrode at different rates are shown in Fig. 4. The discharge capacity at different current rates, e.g. 100 mAg^{-1}, 200

5 mAg^{-1}, 500mAg^{-1}and 1000 mAg^{-1}, are, 991 , 824, 749 and 707 mA h g^{-1}, respectively, indicating a good high-rate performance. The excellent capacity retention may be related to cross linked nanoparticles structure of the materials, which can accommodate the volume change of the Li$^+$ insertion/extraction during the

10 charge -discharge processes, offer a small diameter to enhance lithium diffusion, and yet still provide a limited surface area to prevent excessive side reactions [19].
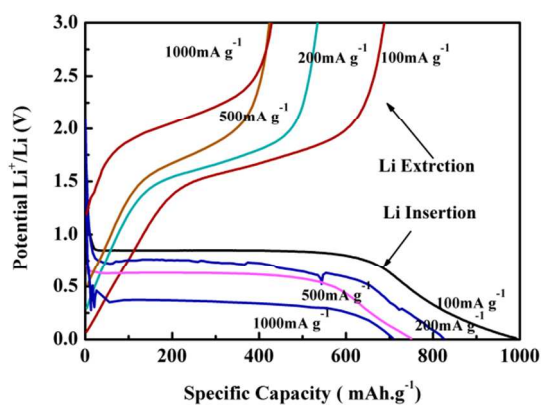

Figure 4 Discharge and charge voltage profiles of the $Li_{0.5}Fe_{2.5}O_4$

15 nanoparticles electrode at different current densities.

Recently, cheap and non-toxic iron-based compounds [20-22], such as Fe_2O_3, Fe_3O_4 and $LiFeO_2$, have been used as anodes for lithium ion batteries, showing excellent electrochemical

20 performances in term of specific capacity, cycle performance and rate capability. The capacity of lithium storage is mainly achieved through the reversible conversion reaction between Li$^+$ and $Li_xFe_yO_z$, forming Fe nanocrystals dispersed in Li_2O matrix. For example, Fe_2O_3 nanotubes showed a highly reversible discharge

25 capacity of 950 mA h g^{-1} in the second cycle and maintained 929 mAhg^{-1} even after 30 cycles, and excellent rate performance (the

918 mAhg^{-1} discharge capacities at 0.5 A g^{-1} current density and 882 mAhg^{-1} discharge capacities at 1 Ag^{-1} current density) [20]. The initial discharge capacity of the carbon nanotubes-66.7wt.%Fe_3O_4

30 nanocomposite electrode is 988 mAh g^{-1}, and its recharge capacity retention after 145 cycles remains 645 mAh g^{-1} [21]. α-$LiFeO_2$-C nanocomposite electrode delivered a good reversible capacity and cycle stability (540 mAh g^{-1} at 848 mA g^{-1} current density after 200 cycles)[11]. The obtained results show that

35 $Li_{0.5}Fe_{2.5}O_4$ nanoparticles anode shows excellent electrochemical properties, inclduing a high capacity in the initial discharge (up to 1124 mAhg^{-1}), a high reversible capacity and good cycle stability (650 mAhg^{-1} after 50 cycles at a current density of 100 mAg^{-1}) and high-rate performance (991 mAhg^{-1} at a current density of

40 100 mAg^{-1}, 707 mA h g^{-1} at a current density of 1 Ag^{-1}).
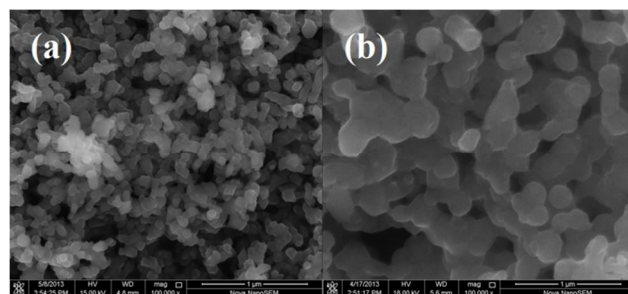
Figure 5 SEM images of lithium ion oxide nanocomposites produced at (a) 500ºC; (b) 700ºC.
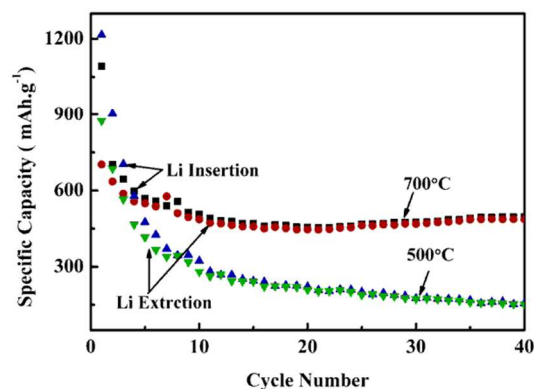
Figure 6. Cycling performances of lithium ion oxide nanoparticles

45 obtained at 500 ℃ and 700 ℃

The morphology and electrochemical performance of the

lithium ion oxide nanoparticles are sensible to the synthesis conditions. As the SEM images in Fig. 5 show the lithium ion oxide nanocomposites produced at different annealing temperatures have the same particle shape but different sizes. The powder produced at 500°C has a smaller particle size of around 70 nm in diameter and a large particle size of 100-200 nm for the sample produced at a high temperature of 700 ^{o}C.

Fig. 6 shows that the sample produced at 700 ^{o}C has the first discharge capacity of 1092mAhg^{-1} and a stable capacity of 500mAhg^{-1}. The nanocomposites obtained at 500℃ demonstrates the first discharge capacity of 1215mAhg^{-1} and a low stable capacity of 200mAhg^{-1}. Therefore, the nanocomposite produced at 600°C has the best electrochemical performance.

Conclusions

Combined hydrothermal and solid state reaction approach has been used to fabricate novel $Li_{0.5}Fe_{2.5}O_4$ nanoparticles with size of 80 nm at 600 ^{o}C. Electrochemical measurements show that $Li_{0.5}Fe_{2.5}O_4$ nanoparticles as anode exhibit a remarkable high capacity in the initial discharge (up to 1124 mAhg^{-1}), a high reversible capacity and good cycle stability (650mAhg^{-1} after 50 cycles at a current density of 100 mAg^{-1}) and excellent coulombic efficiency.

Notes and references

[a] *Beijing Key Laboratory of Energy Nanomaterials, Advance Technology & Materials Co., Ltd, China Iron & steel Research Institute Group, Beijing 100081, P.R. China*

[b] *Institute for Frontier Materials, Deakin University, Waurn Ponds, Victoria 3216, Australia,*

Emails:ian.chen@deakin.edu.au,

References

1 Rotem Marom, S. Francis Amalraj, Nicole Leifer, David Jacob and Doron Aurbach. J. Mater. Chem. , 2011**, 21**, 9938 .

2 Vinodkumar Etacheri, Rotem Marom, Ran Elazari, Gregory Salitra and Doron Aurbach, Energy Environ. Sci., 2011, **4**, 3243.

3 Arumugam Manthiram, J. Phys. Chem. Lett. 2011, **2**, 176.

4 Sagar E. Shirsath, R. H. Kadam, Anil S. Gaikwad, Ali Ghasemi, Akimitsu Morisako, Journal of Magnetism and Magnetic Materials, 2011, **323**,3104.

5 Dongen Zhang, Wenbing Shu, Shanzhong Li, Xiaobo Zhang, Ailing Ying,Zhiwei Tong, Journal of Materials Science, 2008, **43(17)**,5948.

6 Yen-Pei Fu, Cheng-Hsiung Lin, Chung-Wen Liu, Yeong-Der Yao, Journal of Alloys and Compounds, 2005, **395**, 247.

7 Mathew George, Swapna S Nair, Asha Mary John, P A Joy and M R Anantharaman, J. Phys. D: Appl. Phys. 2006, **39**, 900.

8 H M Widatallah, C Johnson, A M Gismelseed, I A Al-Omari, S J Stewart, S H Al-Harthi, S Thomas and H Sitepu, J. Phys. D: Appl. Phys. 2008, **41**, 165006.

9 DongEn Zhang, WenBing Shu, ShanZhong Li, XiaoBo Zhang, Ailing Ying, ZhiWei Tong, J Mater Sci, 2008, **43**,5948.

10 Pier Paolo Prosini , Maria Carewska , Stefano Loreti , Carla Minarini , Stefano Passerini, International Journal of Inorganic Materials , 2000, **2**, 365.

11 Md.Mokhlesur Rahman, Jia-Zhao Wang, Mohd Faiz Hassan, Shulei Chou, Zhixin Chen and Hua Kun Liu, Energy Environ. Sci., 2011, **4**, 952.

12 Shu-Lei Chou, Jia-Zhao Wang, David Wexler, Konstantin Konstantinov, Chao Zhong, Hua-Kun Liu and Shi-Xue Dou, J. Mater. Chem., 2010, **20**, 2092.

13 Bonil Koo, Hui Xiong, Michael D. Slater, Vitali B. Prakapenka, Mahalingam Balasubramanian, Paul Podsiadlo, Christopher S. Johnson, Tijana Rajh, and Elena V. Shevchenko, Nano Lett.2012, **12**, 2429.

14 M. V. Reddy, Ting Yu, Chorng-Haur Sow, Ze Xiang Shen, Chwee Te ck Lim, G. V. Subba Rao, and B. V. R. Chowdari, Adv. Funct. Mater.2007, **17** , 2792.

15 Bing Sun, Josip Horvat, Hyun Soo Kim, Woo-Seong Kim, Jungho Ahn, and Guoxiu Wang, J. Phys. Chem. C, 2010, **114**, 18753.

16 Yong-Mao Lin, Paul R. Abel, Adam Heller, and C. Buddie Mullins, J. Phys. Chem. Lett. 2011, **2**, 2885.

17 Jinping Liu, Yuanyuan Li, Hongjin Fan, Zhihong Zhu, Jian Jiang, Ruimin Ding, Yingying Hu, and Xintang Huang, Chem. Mater. 2010, **22**, 212.

18 Bruce, P. G.; Scrosati, B.; Tarascon, J. M. Angew. Chem., Int. Ed. 2008, **4** , 2930.

19 Tao Tao, Alexey M. Glushenkov, Chaofeng Zhang, Hongzhou Zhang, Dan Zhou, Zaiping Guo, Hua Kun Liu, Qiyuan Chen, Huiping Hu and Ying Chen, J. Mater. Chem., 2011, **21**, 9350.

20 Narae Kang, Ji Hoon Park, Jaewon Choi, Jaewon Jin, Jiseul Chun, Il Gu Jung, Jaehong Jeong, Je-Geun Park, Sang Moon Lee, Hae Jin Kim, and Seung Uk Son, Angew. Chem. 2012, **124**, 6730.

21 Yang He, Ling Huang, Jin-Shu Cai, Xiao-Mei Zheng, Shi-Gang Sun, Electrochimica Acta , 2010, **55**,1140.

22 Jun Song Chen, Ting Zhu, Xiao Hua Yang, Hua Gui Yang, and Xiong Wen Lou, J. AM. CHEM. SOC. 2010, 132, 13162–13164

ARTICLE TYPE

Figure Captions：

Figure. 1 SEM and TEM images (a), and particle size distribution (b) of the sample obtained from Fe_2O_3 and $LiOH \cdot H_2O$ after heating at 600 °C.

5

Figure 2. XRD pattern of samples obtained at 600°C from Fe_2O_3 and $LiOH \cdot H_2O$.

Figure 3(a) Cyclic voltammentry (CV) curves, (b) discharge-charge curves, and (c) cycling performances of $Li_{0.5}Fe_{2.5}O_4$ nanoparticles.

10

Figure 4 Discharge and charge voltage profiles of the $Li_{0.5}Fe_{2.5}O_4$ nanoparticles electrode at different current densities.

Figure 5 SEM images of lithium ion oxide nanocomposites produced at (a) 500^oC; (b) 700^oC.

15

Figure 6. Cycling performances of lithium ion oxide nanoparticles obtained at 500 ℃ and 700 ℃.

20